DOI: 10.13009/EUCASS2022-4922
9TH EUROPEAN CONFERENCE FOR AERONAUTICS AND SPACE SCIENCES (EUCASS)

Analysis of the premixed methane/air flames near to lean blowout in plasma assisted swirl combustor

Bonuso Sara, Mehdi Ghazanfar** and De Giorgi Maria Grazia****
**Department of Engineering for Innovation, University of Salento, Lecce, Italy*
sara.bonuso@unisalento.it
*** Department of Engineering for Innovation, University of Salento, Lecce, Italy*
ghazanfar.mehdi@unisalento.it
**** Department of Engineering for Innovation, University of Salento, Lecce, Italy*
mariagrazia.degiorgi@unisalento.it

Abstract

Lean fuel burning is one of the most prominent methods to achieve low-temperature combustion which reduces a substantial amount of nitrogen oxides (NOx) emissions. However, as a result, strong flame instabilities and very lean operating conditions are associated with the high risk of a lean blowout (LBO). This experimental work investigates the behavior of premixed methane/air flames close to LBO limits at different operating conditions using a plasma-assisted swirl combustor. The combustor was equipped with ring-needle plasma actuator power by a sinusoidal high voltage generator at the maximum frequency of 20 kHz directly coupled with the flame near the nozzle exit. The electrical characterization of plasma-assisted flame was performed at two different fueling conditions by powering the electrode with different voltage amplitudes of the sinusoidal generator. The comparative analysis of LBO stability of baseline case (without plasma) and with different plasma actuation conditions has been performed. The flame behavior was characterized using a high-speed chemiluminescence diagnostic to reveal the spatially and temporally distribution of the flame front and the primary combustion zone. The CH*emissions, which were acquired by an intensified camera equipped with a narrow bandpass filter, were used to analyze the effects of equivalence ratio and plasma actuation on the flame. Proper Orthogonal Decomposition of CH* chemiluminescence images permitted the identification of the dominant flame structures and frequency ranges of the flame fluctuations. A significant improvement in the flame behavior close to the LBO limits was underlined.

1. Introduction

Recently, there is a great interest in the development of aeronautical engines to improve fuel efficiency and reduce nitrogen oxides (NOx) emissions. Lean fuel burning and premixed combustion concepts are considered one of the most attractive techniques to achieve low-temperature combustion. However, as a result, lean burning suffers from severe flame instabilities, and at very lean operating conditions near the flame quenching limit is associated with the high risk of a lean blowout (LBO), which has to be avoided [1]. Therefore, the capability to sense the origin of LBO will provide substantial settlements to improve combustor reliability to achieve optimum performance, extend engine life, and reduce maintenance costs. In this context, passive control methodologies were investigated by changing the combustor and injector geometries in a permanent way, which promoted the flame stability using generating the large-scale vortexes and improving the mixing performance. Besides it, interesting active control technology is given by the use of non-thermal plasma-assisted combustion (NTPAC) [2]. NTPAC technology is the most encouraging technology to actively control the flow and combustion dynamics in real-time operating conditions without altering the combustor design. NTPAC improves the efficiency of combustors, increases flame stabilization, enhances low-temperature oxidation, and extends the LBO limits, in the meantime, it also reduces the significant amount of NOx [3, 4]. The effects of non-thermal plasma (NTP) are broadly classified into three ways: thermal effects, kinetic effects, and transport effects. Among all the NTPAC technologies, the dielectric barrier discharge (DBD) is widely considered, due to the simplicity of its design and the wide range of operating modes [5]. NTPAC is associated with the collisions of high-energy ions and electrons with fuel/air molecules, which breaks the large chains of fuel molecules into radicals

DOI: 10.13009/EUCASS2022-4922

and active species. Adding to this, NTP produced the ionic wind which promoted the mixing performance and stimulated the oxidation reactions. It also increased the contract between the active species and fuel fragments which accelerates the combustion [6]. Recently, some studies have been performed to investigate the LBO limits and flame stabilization. An experimental investigation has been performed by Zare et. al [7] plasma-assisted low-temperature combustion of methane-air flames using a nanosecond pulsed plasma generator. It was perceived that flame stability, ignition delay timings, and LBO limits were improved. Feng et. al [8] investigated the LBO and ignition characteristics using a rotating gliding arc in a swirl combustor. The extension of LBO limits and ignition timings were enhanced. Kim et al [9] studied the impacts of NTP on CO/NOx emissions and LBO limits in a swirl premixed combustor of lean methane/air flames using a DBD reactor. It was concluded that NTP reduced the CO emissions and extended the LBO limits. However, close to LBO conditions, NOx was increased due to ozone, which improved the combustion. Deng [10] investigated the impacts of DBD plasma on the flame instabilities of swirling premixed methane-air flames under acoustic excitation. Dual microphones were used to measure the pressure oscillations. The OH* images and fluctuations of flame transfer function presented the mechanism of plasma actuation in flame instabilities. The flame stability was improved with the increase of OH* concentrations and recirculation zone generated by DBD plasma actuation. Our group also performed some numerical and experimental investigations in a swirl premixed methane/air combustor using a sinusoidal (AC) and nanosecond pulsed plasma generator. The ignition delay timings, flammability limits, and flame speed were investigated [3-4, 11-12]. Smoke flow visualizations and Proper orthogonal decomposition (POD) have been performed to study the dominant flow structures and aerodynamic effects of plasma discharge under quiescent conditions [13-15]. It was noticed that plasma actuation has a significant impact on the production of active particles and fluid dynamics near to burner exit, which ultimately improved the ignition and combustion performance. However, due to the complexities of processes evolved in the NTPAC, the effects of plasma on LBO limits and combustion enhancement are at an exploratory stage. Unfortunately, only a few quantitative experimental studies related to sinusoidally driven plasma-assisted lean methane/air flames were performed. Therefore, for a better understanding of NTPAC processes, this experimental study investigates the behavior of premixed methane/air flames and LBO limits using a plasma-assisted swirl combustor. The combustor was equipped with a ring-needle plasma actuator operated by the sinusoidal generator at the maximum frequency of 20 kHz directly coupled with flame near the nozzle. The electrical characterization of combustion characteristics was performed at different plasma actuation conditions and air/fuel mass flow rates. The comparative analysis of LBO stability of baseline case (without plasma) with different plasma actuation conditions has been performed. The mean value of the dissipated electrical power was calculated for each test. The flame behavior was characterized using a high-speed chemiluminescence diagnostic to reveal the spatially and temporally distribution of the flame front and the primary combustion zone. The emissions, which were acquired by the Phantom M320S camera equipped with a Lambert image intensifier and narrow bandpass filters, were used to analyze the effects of equivalence ratio and plasma actuation on the chemiluminescence from electronically excited (CH*). Proper Orthogonal Decomposition of CH* chemiluminescence images permitted the identification of the dominant frequency ranges in the different operating conditions.

2. Experimental set-up and test cases

The experimental setup consists of a single cup rectangular burner with an area of 105 mm in width and 360 mm in height. The burner is enclosed by transparent quartz glass with a thickness of 2 mm, to provide enough optical access. However, the burner's top is directly opened to the ambient. The fuel and air are fed to the bottom of the combustor controlled by pressure regulators and the gas and airflow meters. The detailed methodology and sketch of the experimental setup are available in our previously published article [11]. An airblast atmospheric nozzle having an effective area of 319 mm^2 is used to produce lifted swirling flames by following the realistic geometrical modeling of aero-combustor. It consisted of two co-rotating swirlers, primary and secondary swirlers to induce rotary movement of air. The primary swirler has eight tangentially inclined vanes with trailing edges that are at a 45° angle to the tube axis when creating a swirl. The secondary swirler is comprised of twelve straight vanes having zero trailing angle. Therefore, the air passing by the secondary swirler hasn't added any additional swirl because not orientated tangentially. These two swirlers are separated from each other by the prefilmer and are met at the edge of the prefilmer and mixed with the fuel. The eight holes in the primary swirler are used to transfer the gaseous fuel to the prefilmer. The experimental system was covered by a faraday cage to stop the intrusion of electromagnetic fields generated with plasma discharge. In particular, the plasma actuator configuration includes a tungsten needle with a length of 46 mm, and a diameter of 1 mm, placed vertically at the central axis of the burner referred to as a high voltage (HV) electrode, while the nozzle acted as a grounded electrode. All the tests were performed under laboratory conditions, a pressure of 1 bar, a humidity of about 60%, and a temperature of about 298 K. Tests were carried out with plasma on and off conditions using different fuel and airflow rates. The experimental conditions and calculated electrical power output is presented in Table 1. Chemiluminescence analysis was performed at a fixed fuel/air equivalent ratio of 0.8 but two

DOI: 10.13009/EUCASS2022-4922

different air flow rate and fuel flow rate values, to see the effect of the inlet reactants velocity, which means inlet Reynolds number.

Table 1: Experimental conditions and calculated electrical power output.

Airflow rate (A_f)	Fuel flow rate (F_f)	Input Amplitude Voltage	Vpp [V]	Vmax [V]	Vmin [V]	Freq [Hz]	P_{el} [W]
6 m^3/h	0.5 m^3/h	40%	5876.8	3082.5	2794.4	19909.1	34
11.5 m^3/h	1 m^3/h	40%	13572.87	6893.9	6678.9	18994.2	73.65

3. Electrical Characteristics and discharge characterization

The electrical set-up consisted of HV sinusoidal amplifier (PVM500 Plasma Resonant), a current transformer (Bergoz CT-D1.0-B), a high voltage (HV) probe (Tektronix P6015A), an oscilloscope, and a personal computer. The HV generator supplies the voltage in sinusoidal waveform V(t) at different amplitudes and a constant frequency of about 20 kHz. The current probe, HV probe, and oscilloscope were used to analyze the temporal evolution of voltage and current and estimate the power consumption. The current probe was placed on the GND side and the HV probe was connected on the HV side, then both probes were connected with an oscilloscope. A detailed sketch of electrical characterization is available in our article [11].

By aiming to increase the measurement accuracy, time-dependent V(t) and I(t) characteristics curves were saved 5 times during the experiment for each test case. The mean value of the electrical power dissipations was calculated for each test by using the following formula:

$$P_{el} = \frac{1}{2T}\int_0^{2T} I(t)V(t)\,dt \qquad (1)$$

The numerical integration has been performed for the power calculation using the trapezoidal rule. The uncertainty analysis of each measured power value was predicted by the standard uncertainty analysis methodology [16].

4. High-Speed Chemiluminescence Flame Imaging and Proper orthogonal decomposition (POD)

In this study, the plasma assisted flame was characterized using a high-speed chemiluminescence diagnostic to reveal the spatially and temporally distribution of the flame front and the primary combustion zone. The emissions, which were acquired by the Phantom M320S camera equipped with a Lambert image intensifier and narrow bandpass filters, was analysed to study the effects of equivalence ratio and plasma actuation on the chemiluminescence from electronically excited methylidyne (CH*) radicals. In particular high-speed images of, CH* signals were acquired. The ICCD camera was coupled with a UV lens of 78 mm with an aperture set at f/3.8. The CH* emission exists in the visible region 380–760 nm where an intense background emission, including soot radiation and CO2*, are present. The CH* chemiluminescence emission were acquired with a 430 nm interference filter. Half of the acquired window, which corresponds to the flame area on the right concerning the central needle (extension 87.5 mm × 155 mm), has been processed to avoid the high light emissions of the central needle. A series of grayscale images are acquired at a framerate of 1000 Hz. At each pixel point, the image gray level value was discretized using 8 bits, ranging from 0 to 255, which respectively define the full dark condition (ultra-low luminosity) and the full bright condition (ultra-high luminosity). The image dataset was processed using Matlab® with user-defined routines. A proper square mask was retrieved and used for the selection of the region of interest (ROI) in the images through cropping operation. Then, the image grayscale was converted to the image luminance ranging between 0 and 1. Proper Orthogonal Decomposition of high-speed acquisitions was implemented for a modal spatio-temporal characterization of the flame, more details are in [17] Briefly, the POD extracts an orthogonal basis of eigenvalues from the generic flow data field decoupling the spatial and temporal contributions, that is

$$g(x;\,t) \;=\; \Sigma_i\, g_i(x;t) \;=\; \Sigma_i\, a_i(t)\,\varphi_i(x) \qquad (2)$$

DOI: 10.13009/EUCASS2022-4922

where the ith temporal eigenfunction represents the ith spatial eigenfunction, and denotes the generic spatial coordinates. The former collects information about the dynamics of the modal coherent structures, the latter consists of a picture of the flow able to capture the scales and shapes of the modal coherent structures. The relative energy contribution in image reconstruction related to the ith POD mode is defined as:

$$\Lambda_i = \frac{\lambda_i}{\Sigma_{j=1}^{N_{POD}} \lambda_j} \qquad (3)$$

where ith is the eigenvalue of the autocorrelation tensor of the flow field data, λ_i = energy of the ith POD mode, and Λi = relative energy of the ith POD mode.

As said in [18], POD can be distinguished based on an approach that uses the combination of averaging and correlation, namely the classic or direct method [19] based on the temporal averaging and spatial correlation, or a second approach that is the snapshot method that uses the spatial averaging and the temporal correlation instead. In this study, the latter has been applied for the analysis of the flame dynamics, since it is suitable when the data field has a good spatial resolution but a relatively short time history. By using this approach, the size of the eigenvalue problem is given by the number of the field snapshots, i.e. NPOD = Nimg.

5. Results and Discussions

5.1 LBO characterization

Flame extinction can arise by lowering the equivalence ratio beyond a minimum threshold limit, which is defined as lean blowout. A stable condition was established throughout the experiments, and then the fuel flow rate was gradually reduced until the flame was extinguished. In particular, the experiment for each condition was repeated three times for the repeatability, and the measurement uncertainty of lean blowout limits was within ±3.5 %. Measurements were made with Mass Flow Meter Bronkhorst D6370 whose uncertainty in flow measurement is ±1.0% reading and ± 0.5% of full scale. The comparative analysis of LBO stability of baseline case (without plasma) with different plasma actuation conditions has been performed. Two different fuelling conditions, at the same fuel/air equivalence ratio were investigated The first one is (m_f=0.5 m^3/h and m_a=6 m^3/h) characterized by lowest air and fuel flow rates. The second one presents m_f=1 m^3/h and m_a=11.5 m^3/h, that means highest inlet Reynolds number. Figure 1 depicts the change in LBO limits when the voltage amplitude was increased. When the plasma was on, significant improvements in the LBO limits were observed for both fueling conditions. At fixed air mass flow rates and slowly reducing the fuel flow rate as in figure 1a, LBO limit was reduced by the rise in the high voltage amplitude, the same effect of the plasma actuation was found in the case of constant fuel flow rate and increasing the air flow rate. The maximum reduction of LBO limits was about 52.77%, when the 40% voltage amplitude plasma (P = 73.65W) was introduced in the burner at m_f=1 m^3/h as shown in Fig 1b. This corresponds to a reduction of the equivalence ratio from 0.66 to 0.37 as compared with the baseline case. However, the increase of the high voltage amplitude from 40% to 60% leads to a slight improvement. However, at the fuelling condition at ma=6 m^3/h the maximum reduction of LBO with plasma was observed as 41.18%.

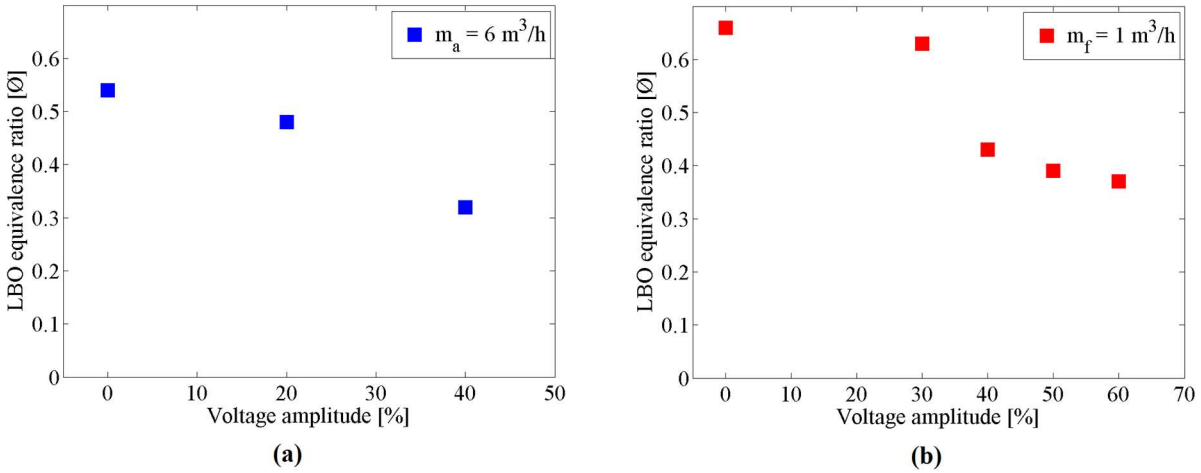

Figure 1: Comparative analysis of LBO limits at different voltage amplitudes (a) fixed m_a = 6 m^3/h and (b) fixed m_f = 1 m^3/h.

DOI: 10.13009/EUCASS2022-4922

5.2 CH* Chemiluminescence and POD analysis

Mean flame structures firstly are analyzed to give an overall impact of plasma actuation on the flame structure. Figure 2 shows the different flame shapes for the studied operating conditions is given by the mean and variance of the CH* signal. Two different fuelling conditions were analyzed. The first fueling condition is (m_f=0.5 m^3/h and m_a=6 m^3/h). The area at high UV emissions increases and moves towards the burner exit if the flame is excited by the plasma discharges, furthermore a slight decrease in the variance is also evident. Then increasing the initial mass flow rates, and fixing the equivalent fuel/air ratio, the chemiluminescence CH* emissions were also measured with and without plasma actuation, as shown in Figure 3. As the fuel and air mass flow rate was increased, the flame region where major heat release occurs moves downstream. Furthermore, it was shown more significant reduction of the flame fluctuations and a wider area with intense heat release for the plasma assisted flame in this last fueling condition.

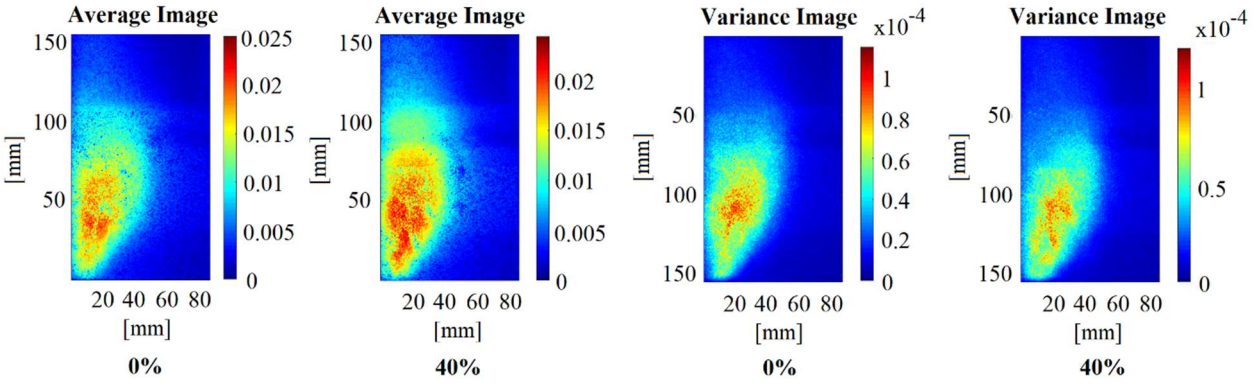

Figure 2. Time-averaged and variance of the CH* chemiluminescence signal (line-of-sight) at m_f=0.5 m^3/h and m_a=6 m^3/h without plasma actuation (0%) and with plasma actuation (Voltage level 40%, Power=34 W).

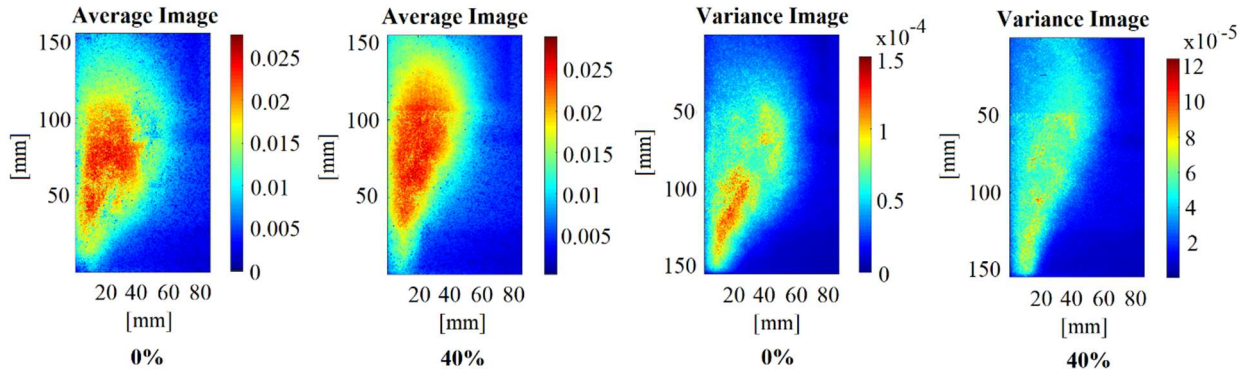

Figure 3. Time-averaged and variance of the CH* chemiluminescence signal (line-of-sight) at m_f=1 m^3/h and m_a=11.5 m^3/h without plasma actuation (0%) and with plasma actuation (Voltage level 40%, Power=73.65 W).

To further understand how the plasma enhances combustion, the POD is employed to identify coherent structures and energetic modes of the flame. POD separates dynamic data into orthogonal modes ordered by decreasing energy, i.e., the lowest order mode is the most energetic. The relative contribution of each mode to the flow field reconstruction is described by their energy. Figure 4 shows the relative energy contributions of the 1-8 eigenmodes (fluctuations). It was noticed that the relative energy is generally distributed by the first 8 modes. It has been observed that in the case of m_f=0.5 m^3/h and m_a=6 m^3/h, the energy content of the first mode is higher than the one of the attached flame. It is evident that with the use of plasma actuation the heat fluctuations of modes 1-8 were significantly decreased in the first few modes. This decreasing energy content for the excited flame is due to the stabilizing effect of the plasma, which leads to lower heat release fluctuations, represented by the energy content in the highest modes.

DOI: 10.13009/EUCASS2022-4922

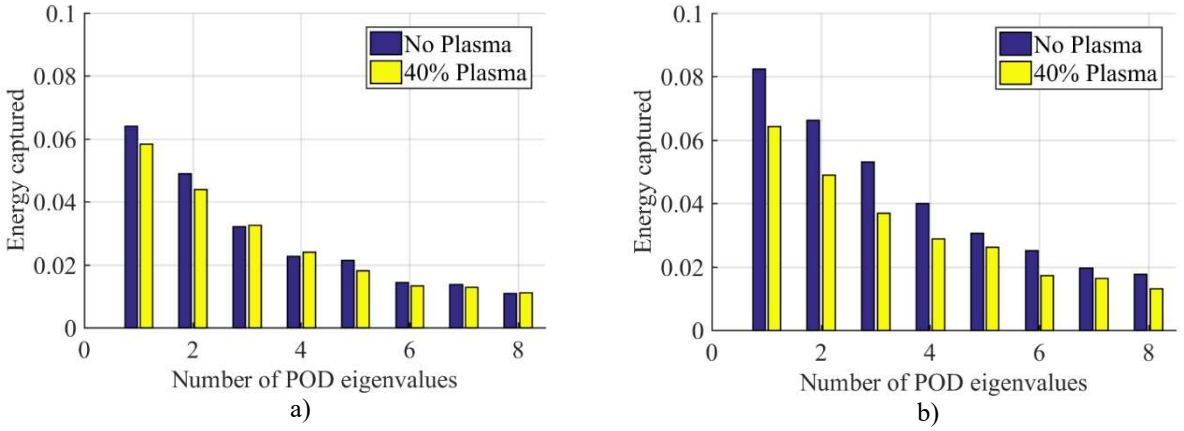

Figure 4: Energy of the details of Proper Orthogonal Decomposition of CH* chemiluminescence images for the case at a) m_f=0.5 m^3/h and m_a=6 m^3/h; b) m_f=1 m^3/h and m_a=11.5 m^3/h

POD was mainly used to determine the coherent structures' frequency and provide information on flame appearance under different fueling and actuation conditions. Figure 5 compares the first 8 POD modes (shown in decreasing energy order) in the case of flame without plasma excitation under the fuelling condition of the m_f=0.5 m^3/h and m_a=6 m^3/h. The scale and the sign of the contour plots representing the mode shapes are arbitrary since the modes are multiplied by their corresponding time coefficients. It should be noted that the modes represent the heat fluctuations, order starting from the most energetic mode (1st mode). Higher modes show coherent structures that can be correlated with flow features. Large-scale vortex structures in the inner mixing layer are clearly visible. These coherent structures are important for studying flame stability. As the mode number increases, the wavenumber of this fluctuations increases. In the flame, without excitation high order modes show large-scale coherent structures that start from the exit of the burner and then develop downstream. The shapes of the first two modes indicate a large axial motion downstream the burner outlet which means that the flame is in the axially dominated movement. The axial motion of the flame fluctuations in the 2nd and 3rd modes, represent an energy content of 20% of the overall energy (calculated as the sum of the energy of all modes). This content is not present in the 4th mode that shows circumferential flame structures and a radial motion. Mode 3 features a wave of alternating positive and negative values across the flame in all operating conditions. However figure 6 shows that the presence of plasma modifies the flame dynamics with a reduction of the width of the flame structures even if their shape is the same for the first 5 modes.

Then fixing the equivalent fuel/air ratio, the mass flow rate of both air and fuel were changed. The POD of CH* chemiluminescence images for the case at m_f=1 m^3/h and m_a=11.5 m^3/h without plasma actuation is shown in Figure 7 and with plasma is shown in Figure 8. It can be seen that the location and modes shape of the heat fluctuation zones change, with larger flow structures, with respect to the previous fueling condition. While the first fueling condition shows a horizonal wave with negative (blue) around positive region (red) for mode 4. As the mass flow rates increase, the radial motion was inhibited due to a strong axial oscillation.

A frequency analysis has been also performed, to identify the main charactestics frequency contents for the different flame structures. As shown in figure 9 the first two modes of the baseline flame without actuation present fluctuations mainly in the low-frequency range, below 100 Hz. A rise of the amplitude of the oscillations at frequency close to 200 and 300 Hz was evident for higher mode numbers, especially mode 3 and 5.

In the plasma assisted combustion the high-frequency fluctuations around 300 Hz are evident in the mode 4, which is an axial motion. The flame excitation by the plasma discharges leads to a decrease of the amplitude fluctuations for all the modes and frequency ranges. This confirms a stabilizing effect of the plasma actuation.

DOI: 10.13009/EUCASS2022-4922

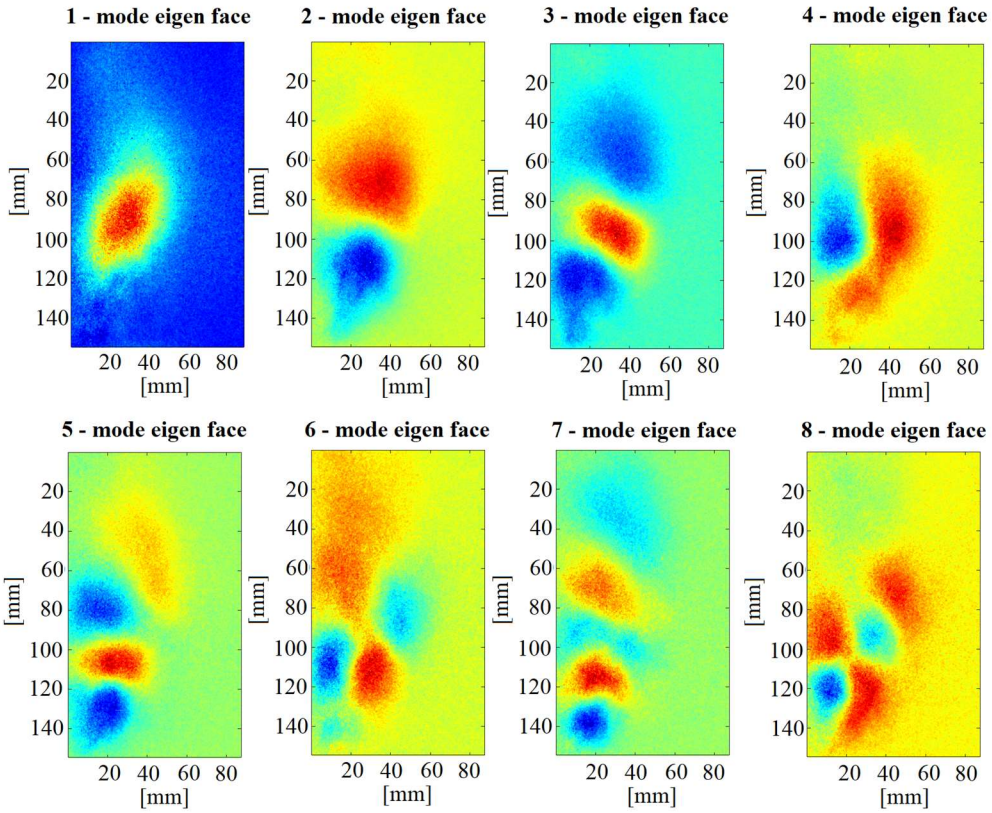

Figure 5. POD of CH* chemilumescence images for the case at m_f=0.5 m^3/h and m_a=6 m^3/h without plasma actuation

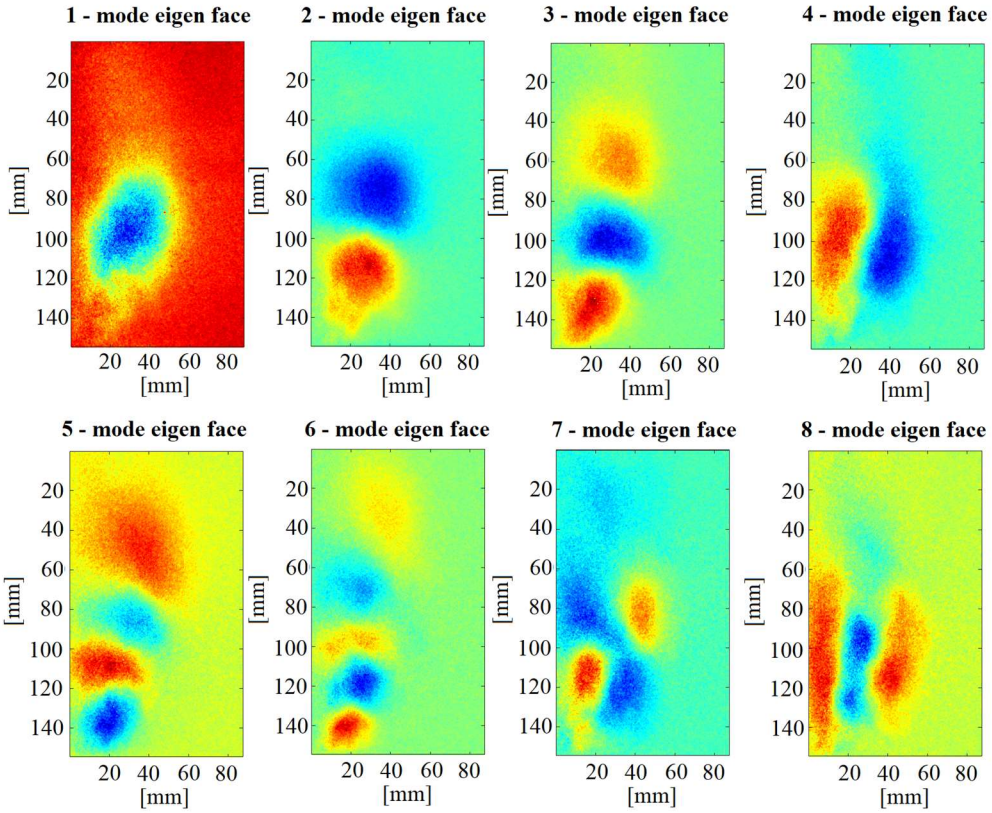

Figure 6. POD of CH* chemilumescence images for the case at m_f=0.5 m^3/h and m_a=6 m^3/h with plasma actuation

DOI: 10.13009/EUCASS2022-4922

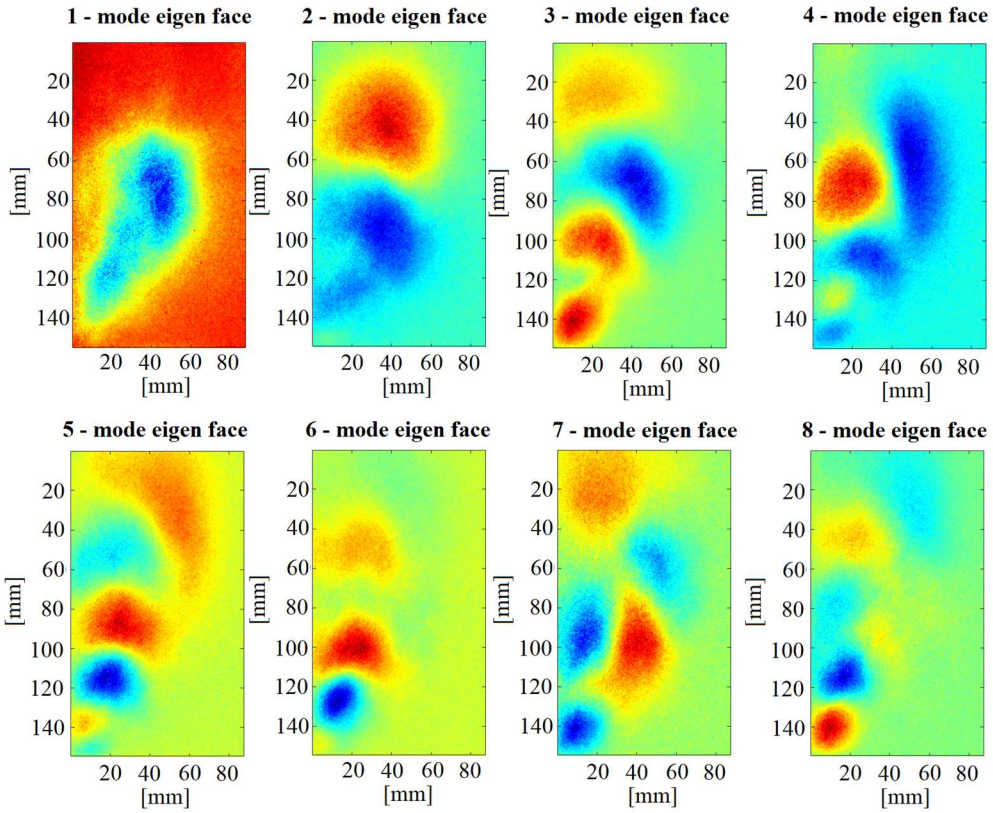

Figure 7. POD of CH* chemiluminescence images for the case at m_f=1 m^3/h and m_a=11.5 m^3/h without plasma actuation.

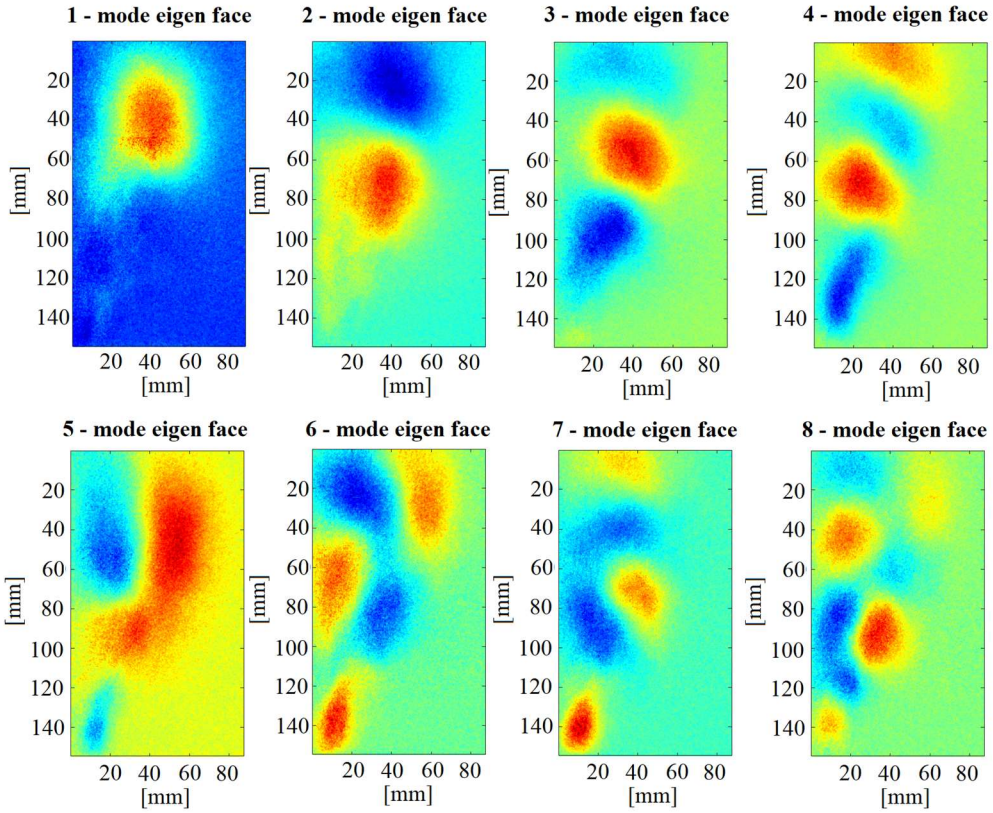

Figure 8. Proper Orthogonal Decomposition of CH* chemilumescence images for the case at m_f=1 m^3/h and m_a=11.5 m^3/h with plasma actuation

DOI: 10.13009/EUCASS2022-4922

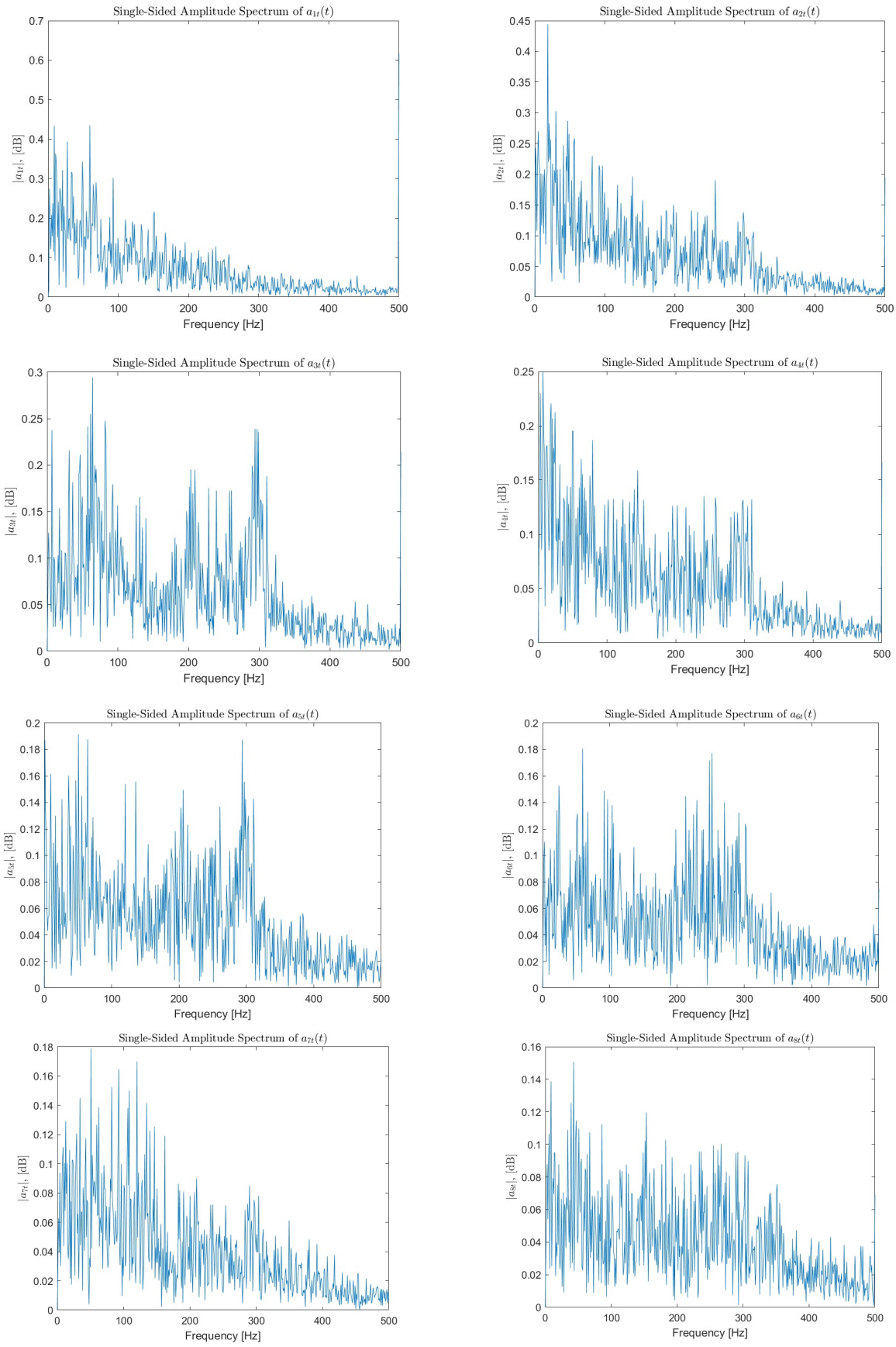

Figure 9. Power spectral density of the time coefficients of the modes of the POD for the case of at m_f=1 m^3/h and m_a=11.5 m^3/h without plasma actuation.

DOI: 10.13009/EUCASS2022-4922

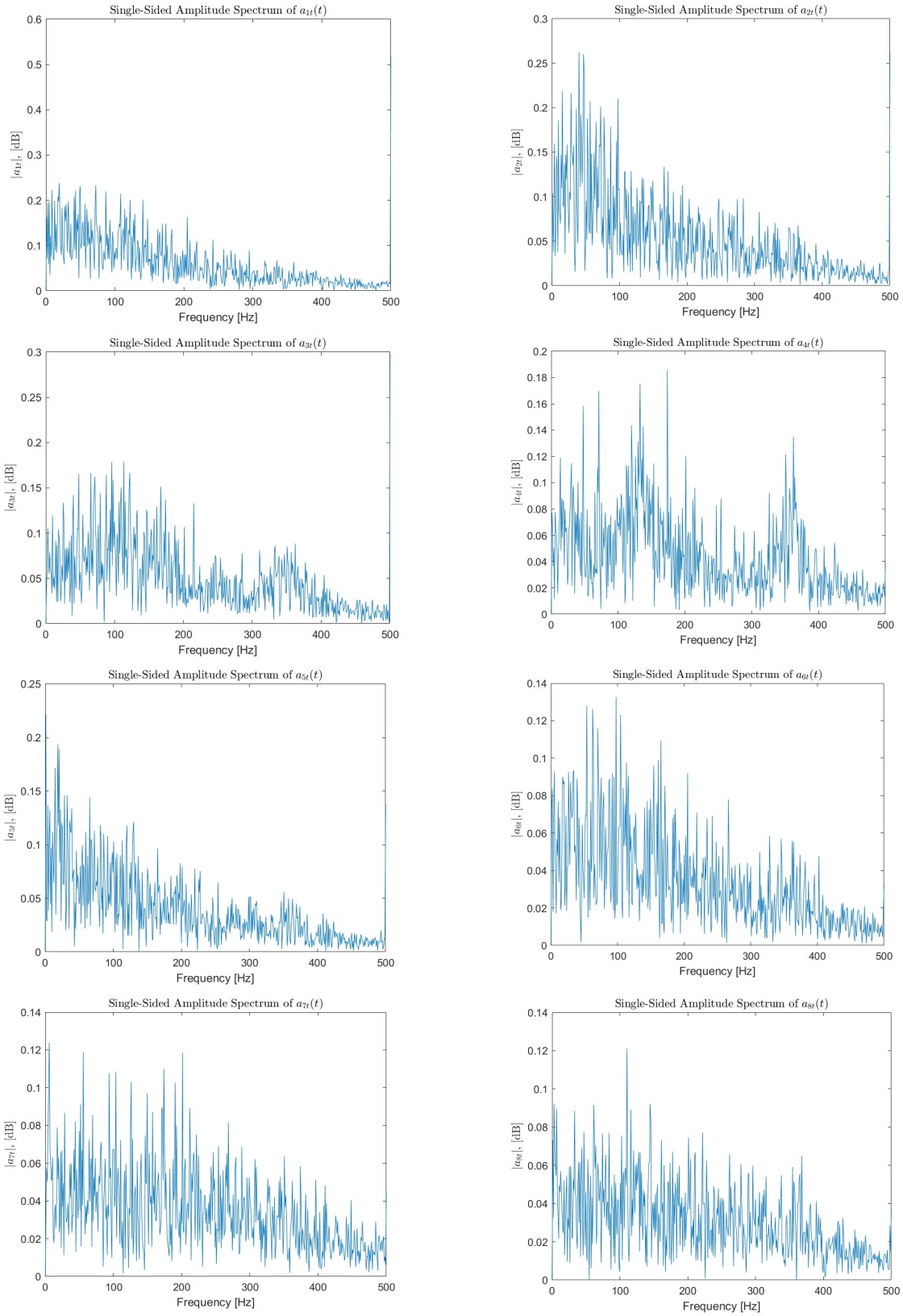

Figure 10. Power spectral density of the time coefficients of the modes of the POD for the case of at m_f=1 m^3/h and m_a=11.5 m^3/h with 40% voltage amplitude of plasma actuation.

DOI: 10.13009/EUCASS2022-4922

6. Conclusions

This study investigates the behavior of premixed methane/air flames close to LBO limits at different operating conditions using plasma-assisted lifted swirl combustor. The burner was equipped with a ring-needle plasma actuator powered by a sinusoidal high voltage generator at the maximum frequency of 20 kHz directly coupled with a flame near the nozzle exit. The electrical characterization of the plasma discharges was performed at two different fueling conditions, which corresponds to different fuel and air Reynolds numbers, by subjecting different voltage amplitudes. The comparative analysis of LBO stability of baseline case (without plasma) and with different plasma actuation conditions has been performed. The flame behavior was characterized using a high-speed chemiluminescence diagnostic to reveal the spatially and temporally distribution of the flame front and the primary combustion zone. Proper Orthogonal Decomposition of CH* chemiluminescence images permitted the identification of the dominant frequency ranges in the different operating conditions. It has been concluded that when the plasma was on, significant improvements in the LBO limits were observed. The maximum reduction of LBO limits was about a percentage of 52.77%, when the 40% voltage amplitude plasma (P = 73.65W) was introduced in the burner at m_f=1 m^3/h and m_a=11.5 m^3/h, as shown in Fig 1b. This corresponds to a reduction of the equivalence ratio from 0.66 to 0.37 as compared with the baseline case. However, the increase of the high voltage amplitude from 40% to 60% leads to a slight improvement. The mean and variance of the CH* chemiluminescence emissions were also analyzed. It has been observed that when the flame was excited by plasma discharge the area at intense CH* emission increases and moves towards the burner exit. Furthermore, a slight decrease in the variance is also evident. Finally, the POD is employed to identify coherent structures and energetic modes of the flame. It was noticed that with the use of plasma actuation axial fluctuation of vortexes was reduced.

Funding: This project has received funding from the Clean Sky 2 Joint Undertaking (JU) under grant agreement No. 831881 (CHAiRLIFT). The JU receives support from the European Union's Horizon 2020 research and innovation programme and the Clean Sky 2 JU members other than the Union.

The work was also supported and funded by the PON R&I 2014– 2020 Asse I ‘Investimenti in Capitale Umano’ Azione I.1 ‘Dottorati Innovativi con caratterizzazione industriale’—Corso di Dottorato in ‘Ingegneria dei Sistemi Complessi’ XXXV ciclo—Universit`a degli Studi del Salento’—Borsa Codice: DOT1312193 n. 3.

Acknowledgments: We thank eng. Sabina Spagnolo for assistance during the construction of the experimental set-up and testing activities.

References

[1] Wollgarten, J.C., Zarzalis, N., Turrini, F., Peschiulli, A. 2017. Experimental investigations of ion current in liquid-fuelled gas turbine combustors, International Journal of Spray and Combustion Dynamics 9(3) 172–185.
[2] Starikovskiy, A., Aleksandrov, N. 2013. Plasma-Assisted Ignition and Combustion. Prog. Ener. Comb. Sci. 39, 61–110.
[3] Fontanaroa, D., Mehdi. G., De Giorgi, M.G., Ficarella. A. 2020. Assessment of the impact of nanosecond plasma discharge on the combustion of methane-air flames, E3S Web Conf. 197 10001 DOI: 10.1051/e3sconf/202019710001.

DOI: 10.13009/EUCASS2022-4922

[4] Mehdi, G., De Giorgi, M.G., Fontanarosa, D., Bonuso, S., Ficarella, A. 2021. Ozone Production with Plasma Discharge: Comparisons Between Activated Air and Activated Fuel/Air Mixture, Proceedings of the ASME Turbo Expo 2021: Turbomachinery Technical Conference and Exposition, 3B: Combustion, Fuels, and Emissions V03BT04A036. ASME. https://doi.org/10.1115/GT2021-60167.
[5] De Giorgi, M.G., Pescini, E., Marra, F., Ficarella, A. 2016. Plasma actuator scaling down to improve its energy conversion efficiency for active flow control in modern turbojet engines compressors. Appl. Therm. Eng. 106, 334–350.
[6] Li, M., Wang, Z., Xu, R., Zhang, X., Chen, Z., Wang, Q. 2021. Advances in plasma-assisted ignition and combustion for combustors of aerospace engines, Aerospace Science and Technology 117:106952.
[7] Zare, S., Lo, H.W., Roy, S., Askari, O. 2020. On the low-temperature plasma discharge in methane/air diffusion flames, Energy 197:117185.
[8] Feng, R., Li, J., Wu, Y., Jia, M., Jin, D. 2020. Ignition and blow-off process assisted by the rotating gliding arc plasma in a swirl combustor, Aerosp. Sci. Technol. 99:105752.
[9] Kim, G.T., Yoo, C.S., Chung, S.H., Park, J. 2020. Effects of non-thermal plasma on the lean blowout limits and CO/NOx emissions in swirl-stabilized turbulent lean-premixed flames of methane/air, Combust. Flame 212: 403–414.
[10] Deng, K., Zhao, S., Xue, C., Hu, J., Zhong, Y., Zhong, Y. 2021 Combustion Instability of Swirl Premixed Flame with Dielectric Barrier Discharge Plasma. Processes 9: 1405. https://doi.org/10.3390/ pr9081405.
[11] De Giorgi, M.G. et al. 2022. Enhancement of Blowout Limits in Lifted Swirled Flames in Methane-Air Combustor by the Use of Sinusoidally Driven Plasma Discharges. In: King, R., Peitsch, D. (eds) Active Flow and Combustion Control 2021. AFCC 2021. Notes on Numerical Fluid Mechanics and Multidisciplinary Design, vol 152. Springer, Cham. https://doi.org/10.1007/978-3-030-90727-3_5.
[12] Mehdi, G., Fontanarosa, D., Bonuso, S., De Giorgi, M.G. 2022. Ignition thresholds and flame propagation of methane-air mixture: detailed kinetic study coupled with electrical measurements of the nanosecond repetitively pulsed plasma discharges, J. Phys. D: Appl. Phys. 55: 315202.
[13] Mehdi, G., Bonuso, S., De Giorgi, M.G. 2022. Plasma Assisted Re-Ignition of Aeroengines under High Altitude Conditions. Aerospace 9, 66. https://doi.org/10.3390/ aerospace9020066.
[14] Mehdi, G., Bonuso, S., De Giorgi, M.G. 2021. Effects of Nanosecond Repetitively Pulsed Discharges Timing for Aeroengines Ignition at Low Temperature Conditions by Needle-Ring Plasma Actuator, Energies 14: 5814, https:// doi.org/10.3390/en14185814.
[15] Mehdi, G., Bonuso, S., De Giorgi, M.G. 2021. Development of plasma actuators for re-ignition of aeroengine under high altitude conditions IOP Conference Series: Materials Science and Engineering, Volume 1226, 012034 International Conference on Innovation in Aviation & Space to the Satisfaction of the European Citizens (11th EASN 2021) 01/09/2021 - 03/09/2021 Salerno.
[16] Pescini, E., Francioso, L., De Giorgi, M.G., Ficarella, A. 2015. Investigation of a micro dielectric barrier discharge plasma actuator for regional aircraft active flow control. Plasma Sci. IEEE Trans. 43(10): 3668–3680 https://doi.org/10.1109/TPS.
[17] Sirovich, l. 1987. Turbulence and the dynamics of coherent structures part iii: dynamics and scaling. Quarterly of Applied Mathematics, 45(3): 583-590.
[18] Kypraiou, A.M., Dowling, A.P., Mastorakos, E., & Karimi, N. 2015. Proper orthogonal decomposition analysis of a turbulent swirling self-excited premixed flame. https://doi.org/10.2514/6.2015-0425.
[19] Lumley, J. L. 1967. The structure of inhomogeneous turbulence. Atmospheric Turbulence and Wave Propagation. AM Yaglom, VI Tatarski, 166-178.